Multi-scale simulations of polymeric nanoparticle aggregation during rapid solvent exchange

Nannan Li, Arash Nikoubashman, and Athanassios Z. Panagiotopoulos

Citation: J. Chem. Phys. **149**, 084904 (2018); doi: 10.1063/1.5046159
View online: https://doi.org/10.1063/1.5046159
View Table of Contents: http://aip.scitation.org/toc/jcp/149/8
Published by the American Institute of Physics

Multi-scale simulations of polymeric nanoparticle aggregation during rapid solvent exchange

Nannan Li,[1] Arash Nikoubashman,[2,a)] and Athanassios Z. Panagiotopoulos[1,a)]
[1]*Department of Chemical and Biological Engineering, Princeton University, Princeton, New Jersey 08544, USA*
[2]*Institute of Physics, Johannes Gutenberg University Mainz, Staudingerweg 7, 55128 Mainz, Germany*

(Received 26 June 2018; accepted 13 August 2018; published online 30 August 2018)

Using a multi-scale approach which combines both molecular dynamics (MD) and kinetic Monte Carlo (KMC) simulations, we study a simple and scalable method for fabricating charge-stabilized nanoparticles through a rapid solvent exchange, i.e., Flash NanoPrecipitation (FNP). This multi-scale approach is based on microscopic information from MD simulations and uses a KMC algorithm to access macroscopic length- and time scales, which allows direct comparison with experiments and quantitative predictions. We find good agreement of our simulation results with the experiments. In addition, the model allows us to understand the aggregation mechanism on both microscopic and macroscopic levels and determine dependence of nanoparticle size on processing parameters such as the mixing rate and the polymer feed concentration. It also provides an estimate for the characteristic growth time of nanoparticles in the FNP process. Our results thus give useful insights into tailoring the FNP technique for fabricating nanoparticles with a specific set of desirable properties for various applications. *Published by AIP Publishing.* https://doi.org/10.1063/1.5046159

I. INTRODUCTION

Colloidal nanoparticles have attracted intensive scientific interest in the past decades because they exhibit many interesting properties suitable for pharmaceutical,[1,2] electronic,[3,4] and photonic[5–7] applications. Since nanoparticle properties and functionalities are primarily determined by parameters such as size, shape, composition, and surface properties, it is highly desirable to develop direct and scalable routes for fabricating colloidal particles with tunable and well-controlled properties.

Here, we model a promising technique named Flash NanoPrecipitation (FNP),[8–11] where a polymer solution is rapidly mixed with an excess amount of a miscible non-solvent to induce aggregation into nanoparticles. Compared to other competing methods, e.g., templating,[12,13] particle lithography,[14,15] or Self-Organized Precipitation (SORP),[16–19] FNP stands out as a one-step continuous process that operates at room temperature, consumes little energy, and has potential to scale up. In addition, it has also been demonstrated both by experiments and by simulations that it is able to access a wide range of structures, including Janus, core-shell,[20,21] patchy,[22–24] and concentric lamellar,[25] using different feed materials, with reliable control over particle size, morphology, and composition. This process can make use of electroneutral polymers with no external stabilizing agents. In this case, the stability of the hydrophobic particles arises from a constant negative ζ-potential between −30 and −40 mV, which was determined from electrophoretic light scattering measurements for the precipitated nanoparticles,[11] and this value is independent of the particle size and polymer chemistry.

Despite the above-mentioned studies aiming to understand and realize the potential of the FNP technique, the underlying microscopic mechanisms are still elusive, as the FNP process takes place on nanometer length scales and nano- to millisecond time scales, which makes the experimental study of the detailed aggregation mechanism difficult. Furthermore, it is an expensive and time-consuming task to systematically search and screen in the experiments all relevant process parameters, such as feed concentration, flow rate, molecular properties, etc.

Computer simulations can provide considerably more microscopic level information than experiments and are therefore efficient tools in the study of complex mechanisms and morphologies. Indeed, the molecular dynamics (MD) model we developed previously[11,20,24,25] has proven to be useful in morphology predictions and producing trends in qualitative agreement with the experiments. Due to computational limitations, however, these MD simulations probed nanoparticles at least 10 times smaller and accessed mixing time scales in the order of a few μs compared to ms employed in the experiments.[11] This gap in length- and time scales prevents quantitative comparisons of experimental data to the MD simulations.

In the present work, we develop a kinetic Monte Carlo (KMC) model, which makes use of the microscopic details obtained from MD simulations, to investigate nanoparticle formation in FNP up to macroscopic length- and time scales by solving stochastically the population balance equation. Other computational approaches capable of reaching experimental scales have also been reported for the study of the FNP process, such as solving the population balance

[a)]Electronic addresses: anikouba@uni-mainz.de and azp@princeton.edu

equation using the method of moments within a computational fluid dynamics code.[26–29] The novelty of the present work consists of the explicit incorporation of the charge stabilization mechanism into the aggregation kernel, which is a key element for studying, e.g., polymers with charged end groups.[10,21] The effect of charge stabilization was not included in previous studies, as they either dealt with nanoparticles stabilized via amphiphilic block copolymers or assumed an aggregation efficiency of either zero or one. Furthermore, our approach allows us to carry out a detailed analysis of the aggregation dynamics and thus to make predictions for important properties relevant to the FNP system, such as the threshold mixing time, the characteristic aggregation time, and the nanoparticle stability from any given set of operating conditions.

The structure of this paper is as follows: we first introduce the simulation model and methods used in the present work in Sec. II. Next in Sec. III, we present our simulation results and focus on understanding the aggregation mechanism and explaining the dependence of nanoparticle size and distribution on processing parameters, such as polymer feed concentrations and characteristic mixing time scale. Finally, in Sec. IV, we summarize our results and comment on their implications on controlled particle production through the FNP process.

II. SIMULATION MODEL AND METHODS

Our simulation model consists of a combination of MD and KMC simulations. The microscopic model used in the MD simulations has already been discussed extensively elsewhere,[11] and therefore we concentrate in this manuscript only on aspects relevant for coupling to the KMC algorithm.

We adopted the KMC algorithm outlined by Gillespie,[30] which has been applied extensively in studying the kinetics of chemical reactions and aggregation processes.[31–35] The KMC simulations can be summarized in the following three major components: (1) an event, k, is chosen to occur so that its probability, $P_k = \frac{K_k}{K_T}$, where K_k and K_T are the rate of event k and the sum of the rates of all possible events for the system at the current time, respectively. (2) The time of the system is advanced by $\tau = -\frac{\ln(u)}{K_T}$, where u is a uniform random number in the interval (0,1]. (3) The system and the rate database are updated.

For the systems of interest for the present work, we consider the relevant events to be particle aggregation due to Brownian diffusion. Nucleation and growth is not included in our description because the aggregation process has been shown experimentally to be growth-controlled.[10] Particle breakage is also assumed to be negligible. In addition, turbulent shear can cause particles to collide and aggregate. Using the turbulent shear kernel outlined by Saffman and Turner,[36] its magnitude only becomes comparable to that of Brownian aggregation for $a \gtrsim 300$ nm. For the range of particle sizes studied in this work, the effect of turbulent shear is thus negligible and therefore has not been considered. The rate constant for Brownian aggregation between particle i and particle j, $K_{i,j}$, can be calculated as follows:[37]

$$K_{i,j} = \frac{4\pi}{W}(a_i + a_j)(D_i + D_j), \tag{1}$$

where a_i and a_j are the radii and D_i and D_j are the diffusion coefficients of particles i and j, respectively. W is the Fuchs stability ratio which takes into account inter-particle interactions,[38]

$$W = (a_i + a_j)\int_{a_i+a_j}^{\infty} \frac{e^{U/k_B T}}{r^2} dr, \tag{2}$$

where U is the total energy of interaction and r is the center-to-center distance between the two particles. $W = 1$ when every collision leads to an aggregation event.

It should be noted that the following assumptions were made with the use of the rate constant in Eq. (1): (a) Particles diffuse toward each other under steady-state conditions. (b) The system is dilute so that only binary collisions are considered. (c) The particle densities are uniform throughout the entire system. (d) Particles are assumed to be spherical.

The state of the KMC system changes after every event, and $K_{i,j}$ needs to be calculated and updated accordingly. To solve for $K_{i,j}$ in Eq. (1), we derived a, D, and W from MD simulations. Since the rate constant, $K_{i,j}$, is derived from MD simulations, the characteristic energy- (ε), length- (σ) and time scales (τ) of the KMC simulations in real units are identical to those of the MD simulations, i.e., $\varepsilon = 4.11 \times 10^{-21}$ J, $\sigma = 1.5$ nm, and $\tau = 0.28$ ns.[11]

The radius of particle i, a_i, can be estimated using

$$a_i = cR_{g,i} = \frac{c\sigma}{2}(N_b N_i)^{\nu}, \tag{3}$$

where $c = 1.3$ from our previous study[11] and $R_{g,i}$ is the radius of gyration of the particle. $\sigma/2$ is the radius of a single bead in the coarse-grained bead-spring MD model used to describe the polymer chains ($\sigma/2 = 0.75$ nm). N_i is the number of chains which belong to particle i, and N_b is the number of beads in a single chain. ν is the Flory exponent, which depends on solvent conditions. For the polystyrene chains with a molecular weight of 16.5 kg/mol studied in the experiments,[11,22,23] our coarse-graining method leads to $N_b = 23$.[11] In addition, the values of ν for different solvent conditions have been calculated from MD simulations and are presented in Fig. 1.

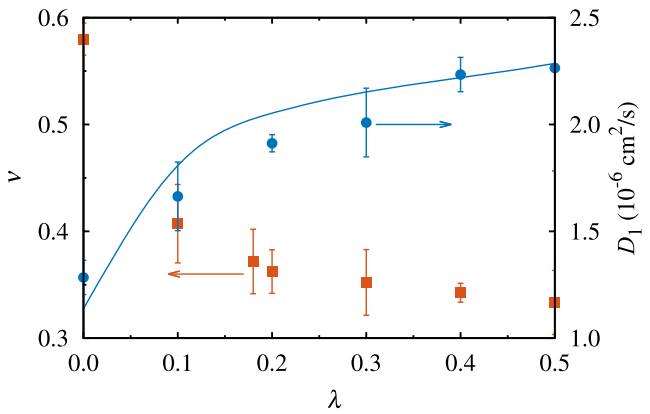

FIG. 1. Dependence of Flory exponent, ν, and diffusion coefficient, D_1, of a single polymer chain of length $N = 23$, on the dimensionless solvent quality parameter, λ, from MD simulations. The line represents predictions from the Stokes-Einstein relation in Eq. (4).

Here, λ is a dimensionless solvent quality parameter in our MD model, which represents the transition from good solvent ($\lambda = 0$) to poor solvent conditions ($\lambda = 0.5$).

The diffusion coefficient of particle i, D_i, can also be calculated from MD simulations. From Fig. 1, it can be seen that the diffusion coefficient of a single polymer chain, D_1, in different solvent conditions shows good agreement with the Stokes-Einstein relation. Therefore, the diffusion coefficient of particle i can be approximated by

$$D_i = \frac{k_\mathrm{B}T}{6\pi\eta_\mathrm{s}a_i}, \tag{4}$$

where k_B is the Boltzmann constant, T is the temperature, and η_s is the dynamic viscosity of the solvent.

Having obtained Eqs. (3) and (4), we now discuss the interaction potentials between the particles, required for calculating, W, in Eq. (2), which will then allow us to obtain the rate constant, $K_{i,j}$, between any given pair of particles. Here, we consider that U is the sum of the van der Waals attraction, U_A, the depletion interaction, U_D, and the electrostatic repulsion, U_R.

In our MD model, the polymer chains consist of Lennard-Jones (LJ) particles that are tethered through massless springs. To reproduce the attractive LJ interaction between the precipitated particles in KMC simulations, we represented U_A as follows:[39]

$$U_{\mathrm{A},i,j}(r) = -\frac{H}{6}\left(\frac{2a_ia_j}{r^2-(a_i+a_j)^2} + \frac{2a_ia_j}{r^2-(a_i-a_j)^2} + \ln\left(\frac{r^2-(a_i+a_j)^2}{r^2-(a_i-a_j)^2}\right)\right), \tag{5}$$

where H is the Hamaker constant and $H = 4\varepsilon\pi^2 = 1.6\times10^{-19}$ J, where 4ε is from the coefficient of the LJ interaction and π^2 arises from integrating all the monomer-monomer interactions over the volumes of the interacting particles. From our MD model, $\varepsilon = k_\mathrm{B}T_\mathrm{room} = 4.11\times10^{-21}$ J, since the experiments were performed at room temperature $T_\mathrm{room} = 298$ K. Values of H calculated for polystyrene in water depend on the methods used and typically lie between 10^{-20} and 10^{-19} J.[40] For our system, we found that the radius of the precipitated nanoparticles, a, is not strongly influenced by the magnitude of H (Fig. S1 in the supplementary material), and a decreased by approximately 10 nm for a 40-fold decrease in H over a broad range of mixing times, while the qualitative behavior remained the same. We have thus used the value of H directly derived from the LJ interaction in all our simulations to be consistent with our MD model. The implication of using this slightly higher H on quantitative comparisons with experiments will be discussed later.

U_D between two spherical particles i and j was approximated by the Asakura-Oosawa model,[41]

$$U_{\mathrm{D},i,j}(r) = \begin{cases} \infty, & r \le 2a_\mathrm{p} \\ -\frac{4P\pi(a_\mathrm{s}+a_\mathrm{p})^3}{3}\left[1-\frac{3r}{4(a_\mathrm{s}+a_\mathrm{p})}+\frac{r^3}{16(a_\mathrm{s}+a_\mathrm{p})^3}\right], & 2a_\mathrm{p} < r < 2a_\mathrm{p}+2a_\mathrm{s} \\ 0, & 2a_\mathrm{p}+2a_\mathrm{s} \le r, \end{cases} \tag{6}$$

where a_p is the mean radius of particles i and j and a_s is the radius of solvent particles ($a_\mathrm{s} = 0.75$ nm in our MD model). P is the osmotic pressure, and $P = \rho_\mathrm{s}k_\mathrm{B}T$, where ρ_s is the number density of solvent particles and $\rho_\mathrm{s} = 0.2$ nm^{-3} from our MD model.

The third component of U is the screened electrostatic repulsion U_R. We adopted the Yukawa potential[42] used in our MD model

$$U_{\mathrm{R},i,j}(r) = \lambda_\mathrm{B}\left(\frac{Z_ie^{\kappa a_i}}{1+\kappa a_i}\right)\left(\frac{Z_je^{\kappa a_j}}{1+\kappa a_j}\right)\frac{e^{\kappa r}}{r}, \tag{7}$$

where λ_B is the Bjerrum length and κ is the inverse Debye screening length, λ_D. For water with pH = 7 at room temperature, we used $\lambda_\mathrm{B} = 0.7$ nm and $\lambda_\mathrm{D} = 0.15$ μm. The parameter Z_i denotes the size-dependent charge of particle i, which can be estimated using Gauss's law for a spherically symmetric environment within linear-screening theory and at low particle concentrations,

$$Z_i = \frac{(1+\kappa a_i)a_ie\zeta}{\lambda_\mathrm{B}k_\mathrm{B}T}, \tag{8}$$

where ζ is the zeta potential, and $\zeta \approx -30$ to -40 mV from experimental measurements using electrophoretic light scattering. For more details on obtaining the values of these parameters, we refer the reader to Ref. 11.

The effect of solvent displacement was accounted for in our KMC simulations in the following two aspects. First, we varied parameters such as λ_B, κ, and ζ between their values for good solvent conditions and poor solvent conditions linearly within a certain period of time, τ_mix. This procedure mimics the effect of increasing surface potential when the polymer solution in the good solvent is rapidly mixed with water. A larger τ_mix corresponds to slower mixing in the experiments and vice versa. It should be noted that in the experiments, the mixing time scale is controlled by the flow rates of the inlet streams. The micromixing time of the multi-inlet vortex mixer used in the experiments has been studied using competitive reactions, and it was found to be in the range of milliseconds for the Reynolds number larger than 1600.[8,9] This quantity is the characteristic time scale for molecular diffusion across fluid lamellae during mixing. Note, however, that the mixing time in our simulations has a slightly different physical

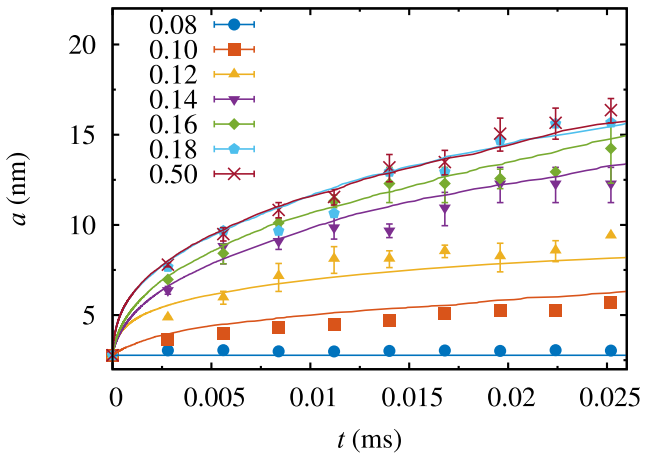

FIG. 2. Average radius of nanoparticles, a, vs. time, t, for different λ values from MD simulations (points) and KMC simulations (lines), which used a linearly increasing prefactor, f. There is no electrostatic repulsion between aggregates in these simulations.

meaning: here, τ_{mix} can be understood as the time before the surrounding non-solvent to solvent ratio has reached its final value in the non-solvent reservoir and surface charge is fully built up. Therefore, τ_{mix} cannot be compared directly to the experimentally measured quantity in Refs. 8 and 9. However, τ_{mix} studied in our simulations still reflects the rate of mixing in the experiments and can provide useful insights into aggregation dynamics and the characteristic aggregation time required to obtain nanoparticles of a certain size as will be shown in Sec. III.

Second, the effect of solvent quality should also be reflected in the effective inter-particle interaction, U. For example, in Θ conditions, which occur at approximately $\lambda = 0.05$ for our model, the LJ interaction between monomers is identical to the monomer-solvent interaction, and the chains are effectively inert to one another. We have studied polymer chain aggregation using MD simulations for different λ values, and the average particle size, a, *vs.* time, t, is shown in Fig. 2. It can be seen that for $\lambda \leq 0.08$, no aggregation occurred despite the presence of van der Waals attraction between polymer chains. The aggregation rate then increased gradually for increasing λ until it reached its full value for $\lambda \geq 0.18$. To account for this solvent effect in our KMC model, we modified the aggregation rate constant, $K_{i,j}$, by a prefactor, f, so that $f = 0$ for $\lambda \leq 0.08$, and $f = 1$ for $\lambda \geq 0.18$. In the intermediate region for $0.08 < \lambda < 0.18$, f increases linearly from 0 to 1. This modification of the KMC aggregation rate constant produced good agreement with MD simulations as shown by the comparison shown in Fig. 2.

III. RESULTS

We first verified our KMC model by comparing aggregation dynamics from KMC with results from MD. In Fig. 3, we plot the time evolution of the average particle radius, a, for polymer feed concentration, $\Phi = 8.2$ mg/mL and different τ_{mix} and ζ values in panels (a) and (b), respectively. Good agreement between KMC and MD results can be seen in all cases, except for small τ_{mix} value of 7 μs [dotted line in Fig. 3(a)].

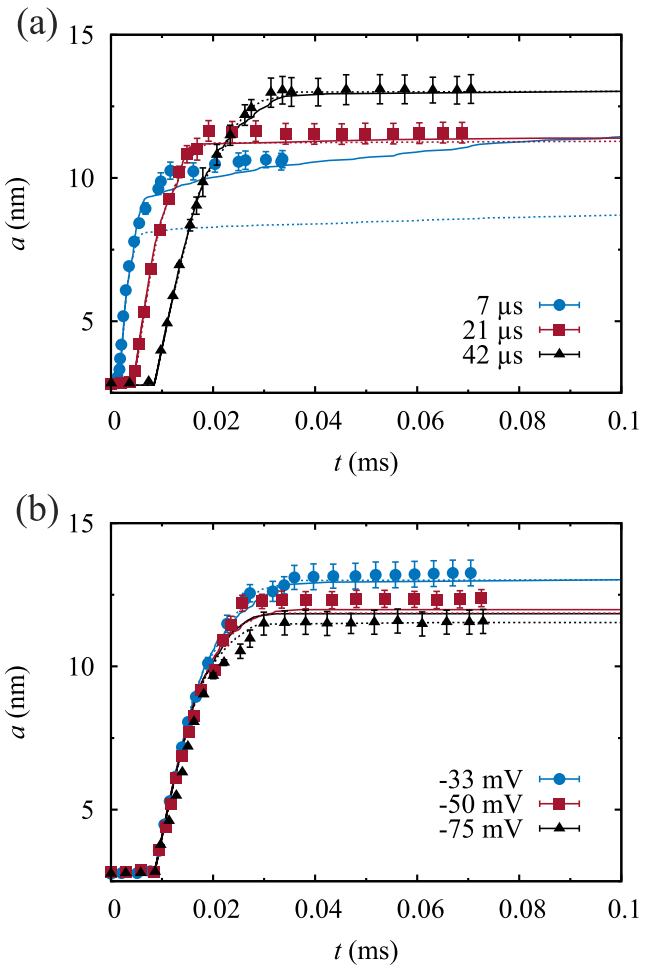

FIG. 3. Average nanoparticle radius, a, vs. time, t, from MD and KMC simulations for polymer feed concentration of 8.2 mg/mL and (a) −33 mV and different τ_{mix} values, and (b) τ_{mix} = 42 μs and different ζ values. The points are from MD simulations. The solid lines and dotted lines are from KMC simulations with and without corrections for the stability ratio, respectively.

This discrepancy arises from the stability ratio, W, which assumes that particles approach each other from infinity with zero interaction. However, for large Φ and small τ_{mix}, high surface charge is fully built up when there are still many small particles in the system and particles do not approach each other from zero interaction due to the long-ranged nature of the electrostatic repulsion. A correction to W was applied so that the integral in Eq. (2) was bounded between $[a_i + a_j, l]$. l is the mean free path between the particles and can be estimated as $l \approx \rho_{\text{p}}^{-1/3}$, where ρ_{p} is the number density of the precipitated particles in the system. It can be seen that better agreement for τ_{mix} = 7 μs was achieved as shown in Fig. 3(a). However, such a correction to the KMC algorithm is only required for comparisons with the high Φ and small τ_{mix} employed in our previous MD simulations.[11] By contrast, typical FNP experiments operate in the range of much smaller Φ (<1 mg/mL) and larger τ_{mix} (>100 μs). It can be seen from Fig. 3 that in this case, the particle concentration of the system is low when surface charge is fully built up and the assumption that particles approach each with zero interaction becomes valid.

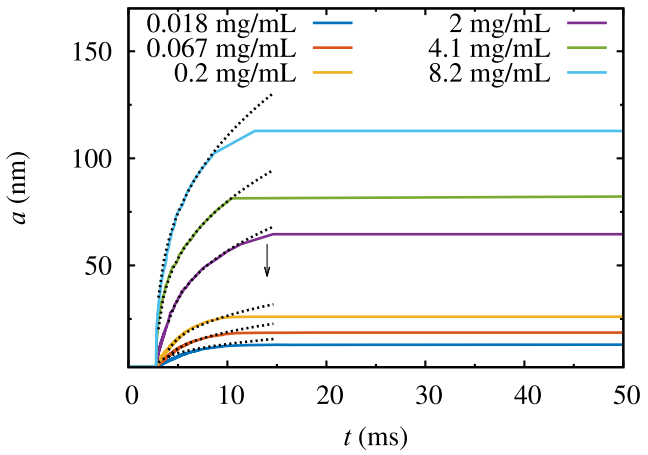

FIG. 4. Average nanoparticle size, a, vs. time, t, for τ_{mix} = 14 ms and ζ = −33 mV. The dotted lines are fits to the DLA approximation. The arrow marks the completion of mixing.

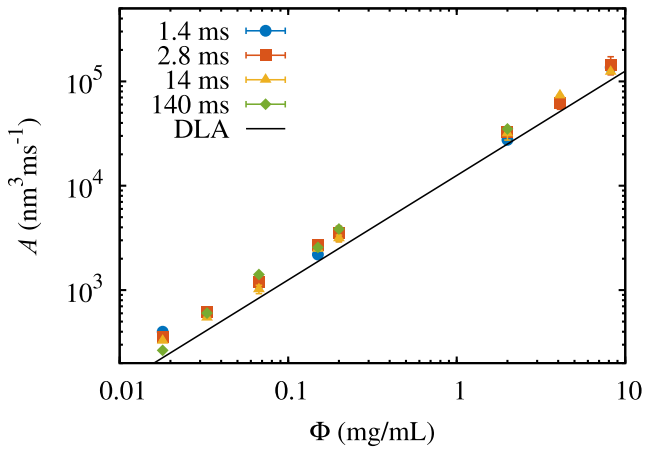

FIG. 5. Fitted parameter, A, vs. Φ from KMC simulations for ζ = −33 mV and different τ_{mix} values. The solid line shows predicted A from the DLA approximation.

Having verified the agreement of the KMC model with our previous MD simulations, we first studied the aggregation mechanism by plotting nanoparticle radius, a, *vs.* t for τ_{mix} = 14 ms and ζ = −33 mV and different polymer feed concentrations in Fig. 4. To describe the time evolution of a at short times, we consider the diffusion limited aggregation (DLA) dynamics.[43] The DLA model gives the change in the average aggregation number, N, with respect to time, t, according to

$$N = 1 + \frac{1}{2} K_{\text{DLA}} \Phi t, \tag{9}$$

where Φ is the initial concentration. K_{DLA} is the rate kernel from the DLA approximation, and

$$K_{\text{DLA}} = 16\pi a_1 D_1, \tag{10}$$

where a_1 and D_1 are the radius and diffusion coefficient of a single polymer chain defined by Eqs. (3) and (4), respectively. Equation (10) assumes W = 1, and the rate kernel for aggregation is independent of particle size. It is a good approximation for aggregation between particle i and j when $1 < m_i/m_j < 2$, where m_i and m_j are the masses of particles i and j, respectively.

To compare our KMC results to DLA approximation, we fit the data in Fig. 4 using the relationship $a = (At + B)^{1/3}$, since $a \propto N^{1/3}$ for spherical close-packed particles. It can be seen that at short times before mixing is complete, the time evolution of a can be well described by DLA. The reason is twofold. First, there is a large number of similarly sized particles in the early stage of aggregation, and the condition $1 < m_i/m_j < 2$ can be satisfied for most of the aggregation events that take place. Therefore, the $(a_i + a_j)(D_i + D_j)$ term in Eq. (1) is approximately constant. Second, at the early stage of aggregation when the electrostatic repulsion is still small, W is also close to 1. The dynamics can thus be approximated by a constant $K_{i,j}$ and fitted through the relationship $a = (At + B)^{1/3}$.

When we plot A *vs.* Φ in Fig. 5; the data can be fitted through a relationship $A \propto \Phi^b$, where b = 0.98 ± 0.02. This scaling relationship is in good agreement with predictions from DLA, i.e., $A \propto \Phi$. However, as shown in Fig. 5, the values of A calculated from DLA are slightly smaller than the fitted values because at the early stage of aggregation when the electrostatic repulsion is small, W is dominated by attractive potentials, i.e., U_{A} and U_{D}, and W is smaller than 1. Aggregation is thus slightly faster than DLA predictions, which assume W = 1.

As mixing proceeds and surface charge builds up on the precipitated nanoparticles, aggregation enters a slow-growth regime and deviates from the DLA approximation. In Fig. 6,

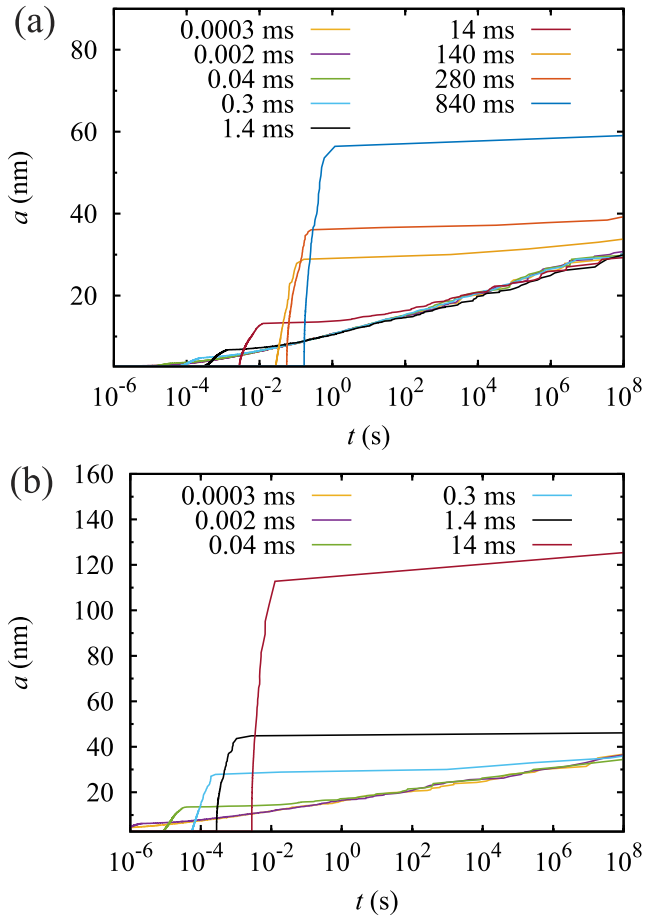

FIG. 6. Average nanoparticle radius, a, vs. time, t, for (a) 0.018 mg/mL and (b) 8.2 mg/mL for different τ_{mix}. The ζ-potential is −33 mV. Growth curves for τ_{mix} > 14 ms are not shown in (b) for clarity because they lead to much larger a values.

a is plotted against t up to macroscopic time scales for two different Φ values. It can be seen that small nanoparticles are less stable after mixing is complete and they continue to grow at a slower rate and gradually converge on a much larger time scale. To understand the convergence, we consider the rate of aggregation. Unlike the rate of aggregation in the DLA regime [Eq. (9)], which is directly proportional to Φ as K_{DLA} is constant, the rate of aggregation in the slow growth regime is largely determined by the magnitude of W. Smaller particles as a result of smaller τ_{mix} or Φ experience a weaker electrostatic repulsion, which leads to a smaller W and higher rate constant, and vice versa. Therefore, growth curves for different τ_{mix} and Φ in Fig. 6 eventually converge to a similar value of a when they are allowed to evolve in the slow growth regime for a sufficiently long time. By contrast, larger particles are more strongly stabilized by charge, and their growth is less appreciable on macroscopic time scales up to 10^8 s. This observation is consistent with experimental measurements, which indicate a 10% to 15% increase in radius for nanoparticles obtained from FNP with $a > 50$ nm after one month.[44]

From Fig. 6, it can be seen that for any chosen cut-off time, t_{f}, growth curves of a below a threshold τ_{mix} value converge. We thus define the threshold τ_{mix} as τ_{thr}. We are interested in τ_{thr} because for $\tau_{\mathrm{mix}} \leq \tau_{\mathrm{thr}}$, a calculated at t_{f} is independent of τ_{mix}. Experimentally, this finding suggests that there exists a threshold mixing rate, and any further increase in this rate does not produce smaller nanoparticles. It is evident that τ_{thr} depends on the t_{f} value chosen. For larger t_{f}, more growth curves converge within the given time, which means larger τ_{thr}. Furthermore, it can be seen from Fig. 6 that larger Φ leads to smaller τ_{thr}. This is because larger Φ results in higher aggregation rate in the DLA regime and larger difference in a for different τ_{mix} values at the start of the slow growth regime. Fewer growth curves thus converge within the given time.

To understand the dependence of τ_{thr} on different parameters, we plot τ_{thr} for two different t_{f} values in Fig. 7. As expected, τ_{thr} increases with decreasing Φ and increasing t_{f}. On the other hand, τ_{thr} can also be predicted from the DLA model. It can be seen from Fig. 6 that for a given t_{f} value, there is a minimum a, a_{thr}, that cannot be undercut by further decrease in τ_{mix}. τ_{thr} is thus the characteristic growth time in the DLA regime to form a particle of radius a_{thr}. Using the fitted parameters A and B we obtained previously, we plot predictions from the DLA approximation in Fig. 7, and they show good agreement with τ_{thr} obtained from performing multiple KMC simulations for different τ_{mix} values.

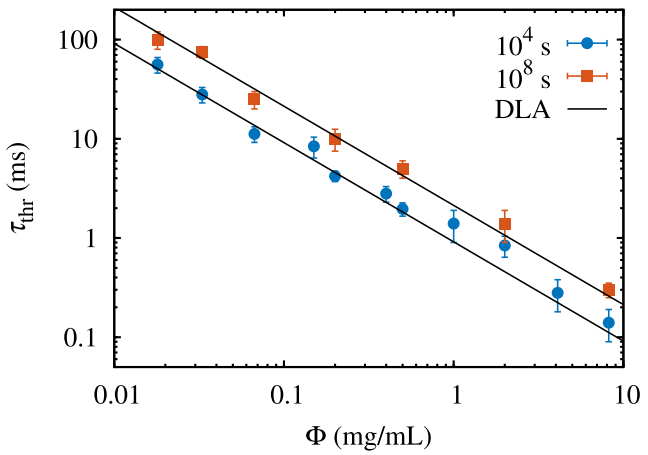

FIG. 7. Threshold mixing time, τ_{thr}, for two different t_{f} values from KMC simulations. The solid lines are approximations from DLA.

Having understood the aggregation dynamics, we then performed KMC simulations for more τ_{mix} and Φ values, and results are shown in Fig. 8(a). Values of a were calculated at a "final" time, t_{f}, arbitrarily set to 10^4 s. The choice of t_{f} affects the minimum nanoparticle radius, a_{thr}. However, it does not affect significantly a for $\tau_{\mathrm{mix}} > \tau_{\mathrm{thr}}$, since larger τ_{mix} leads to larger a, which is stabilized up to 10^8 s as shown in Fig. 6.

Several features of the aggregation process can be observed from Fig. 8. (a) Nanoparticle radius, a, increases with τ_{mix} because the particles stay longer in the DLA growth regime before charge builds up and slows down growth significantly. (b) a increases with Φ for a given τ_{mix} above its corresponding τ_{thr} because a is dictated by growth in the DLA regime for $\tau_{\mathrm{mix}} > \tau_{\mathrm{thr}}$. As shown in Eq. (9), larger Φ leads to larger particles in this regime. (c) Below τ_{thr}, the initial concentration, Φ, has little effect on the final a because the t_{f} chosen, i.e., 10^4 s, is much larger than τ_{mix}. In other words, particles stay much longer in the slow growth regime than in the DLA regime. The initial difference in size as a result of

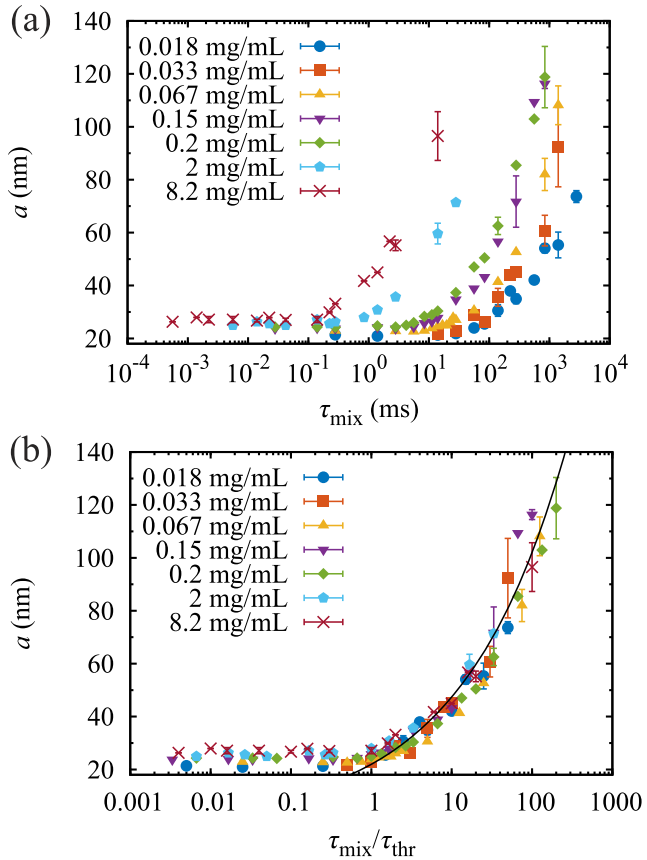

FIG. 8. Average nanoparticle radius, a, vs. (a) τ_{mix} and (b) τ_{mix} reduced by τ_{thr}, for different Φ and −33 mV. Values of a were measured at $t_{\mathrm{f}} = 10^4$ s. The solid line represents $a \propto (\tau_{\mathrm{mix}}/\tau_{\mathrm{thr}})^{1/3}$.

different Φ in the DLA regime becomes insignificant and particles eventually converge to a similar size. These trends are in qualitative agreement with previous studies on the self-assembly of amphiphilic block copolymers using FNP,[45] which also involves fast unimer addition, followed by a much slower aggregate fusion process due to the formation of coronas of overlapping soluble brushes.

In addition, if a is plotted against τ_{mix} reduced by its corresponding τ_{thr} in Fig. 8(b), all data collapse onto the same master curve. For $\tau_{mix}/\tau_{thr} > 1$, the data can be fitted through a relationship $a \propto (\tau_{mix}/\tau_{thr})^c$, where $c = 0.3 \pm 0.02$. The scaling relationship can be explained by the DLA growth model, which predicts $a \propto t^{1/3}$ for spherical close-packed particles.

Finally, we compare the dependence of a on Φ from KMC simulations to experimental measurements. A multi-inlet vortex mixer was used for the experiments, which contained four inlet ports controlled by digital syringe pumps and a single effluent stream. Mixing was performed at a rate which led to a Reynolds number of approximately 2200. More details on the experiments can be found in Ref. 11. In Fig. 9, it can be seen that results from simulations obtained for $\tau_{mix} = 850$ ms and $\zeta = -33$ mV are in quantitative agreement with those from the experiments[11] and a increases with Φ according to a relationship $a \propto \Phi^{1/3}$. Therefore, our KMC model deduced that for the particle sizes obtained in the experiments, the characteristic growth time is approximately 850 ms, which can also be interpreted as the time it takes for the non-solvent to solvent ratio to reach its final value in the non-solvent reservoir in the experiments. However, since the Hamaker constant used in our simulations is at the upper end of the range of values calculated for the experimental system, the actual characteristic growth time can be higher than 850 ms. The lowest Hamaker constant reported for polystyrene in water is approximately 10^{-20} J,[40] which, according to our KMC approach, leads to an upper limit for the characteristic growth time of approximately 1 s. This 18% increase in time as a result of a more than 10 times decrease in H shows that the size of the precipitated nanoparticles is not strongly influenced by the value of the Hamaker constant used in our simulations. It has

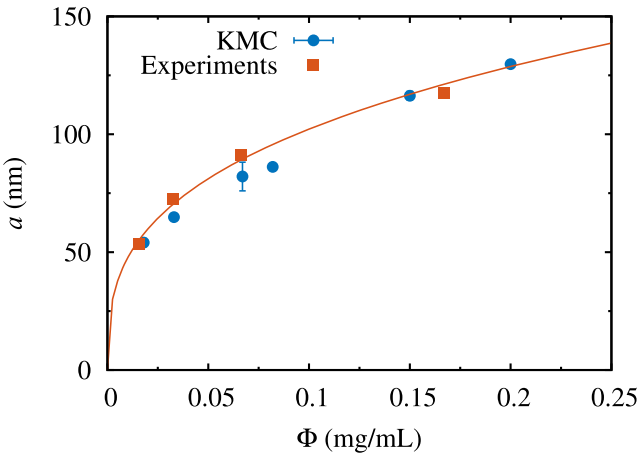

FIG. 9. Average radius of nanoparticles, a obtained from the experiments and from KMC simulations for $\tau_{mix} = 850$ ms, $\zeta = -33$ mV, and different concentrations. The solid line is the fit to experimental data, which represents $a \propto \Phi^{1/3}$.

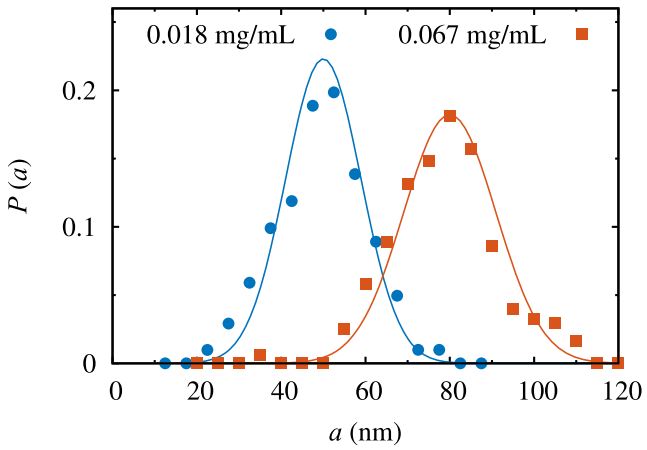

FIG. 10. Size distributions for nanoparticles obtained for $\Phi = 0.018$ mg/mL and 0.067 mg/mL, $\tau_{mix} = 850$ ms and $\zeta = -33$ ms from KMC simulations. The lines are Gaussian distribution fits.

been previously estimated in the experiments that, for systems of hydrophobic core material and amphiphilic block copolymer, the FNP mixer can achieve homogenous mixing on the order 1.5-3 ms.[8] Subsequent assembly of the supersaturated core material and hydrophobic block of the copolymer follows diffusion-limited aggregation, and characteristic particle formation time occurs on the order of 10-100 ms.[45,46] However, nanoparticles obtained from homopolymers undergoing FNP, which are stabilized by a constant ζ-potential have not been studied previously. Our KMC simulations provide insights into the characteristic time scale of this process.

Figure 10 shows the size distribution of the precipitated nanoparticles for $\zeta = -33$ ms, $\tau_{mix} = 850$ ms, and $\Phi = 0.018$ and 0.067 mg/mL. Results from KMC can be fitted through Gaussian distributions, with standard deviations of approximately 15%, which are also in good agreement with experimental measurements.[11]

IV. CONCLUSIONS

In summary, we have developed a multi-scale model, which combines both MD and KMC simulations and allows us to simulate the formation of charge-stabilized polymeric nanoparticles through rapid solvent exchange up to macroscopic length- and time scales. This model is derived based on microscopic details from MD simulations and produces results which are in quantitative agreement with experiments.

Based on the results from our simulations, we were able to elucidate the aggregation mechanism, consisting of a fast growth regime when the surface charge is still small, which can be approximated by the DLA mechanism, and a slow growth regime when the surface charge is fully built-up. For slow mixing, nanoparticles stay longer in the DLA regime and are mostly stabilized in the subsequent slow growth regime. Therefore, nanoparticle size can be predicted from the DLA approximation. On the other hand, for fast mixing, growth in the DLA regime is small. Nanoparticle sizes are thus dictated by the slow growth regime, and they eventually converge over macroscopic time scale; i.e., size is independent of the mixing rate and feed concentration. From our simulations, we have also derived and explained the dependence of nanoparticle size on

processing parameters, e.g., polymer feed concentration and characteristic mixing time scale. This knowledge demonstrates that the rapid mixing of a polymer solution with a non-solvent through FNP produces uniformly sized nanoparticles with reliable control. Together with our previous MD studies,[20,24,25] our results allow us to predict the range of operating conditions required to obtain nanoparticles of a certain size and morphology and thus provide useful guidelines for fabricating nanoparticles with desired properties for applications in various areas.

SUPPLEMENTARY MATERIAL

See supplementary material for the dependence of nanoparticle radius on the Hamaker constant.

ACKNOWLEDGMENTS

Financial support for this work was provided by the Princeton Center for Complex Materials (PCCM), a U.S. National Science Foundation Materials Research Science and Engineering Center (Grant No. DMR-1420541). Furthermore, N.L. acknowledges funding from Agency for Science, Technology, and Research (A*STAR), Singapore. A.N. acknowledges funding from the German Research Foundation (DFG) under Project No. NI 1487/2-1.

[1] R. Langer and D. A. Tirrell, Nature **428**, 487 (2004).
[2] J. A. Champion, Y. K. Katare, and S. Mitragotri, Proc. Natl. Acad. Sci. U. S. A. **104**, 11901 (2007).
[3] C. M. Liddell, C. J. Summers, and A. M. Gokhale, Mater. Charact. **50**, 69 (2003).
[4] X. Wang, C. J. Summers, and Z. L. Wang, Nano Lett. **4**, 423 (2004).
[5] H. Fudouzi and Y. Xia, Adv. Mater. **15**, 892 (2003).
[6] M. Grätzel, Nature **414**, 338 (2001).
[7] C. Liddell and C. Summers, J. Colloid Interface Sci. **274**, 103 (2004).
[8] B. K. Johnson and R. K. Prud'homme, AIChE J. **49**, 2264 (2003).
[9] Y. Liu, C. Cheng, Y. Liu, R. K. Prud'homme, and R. O. Fox, Chem. Eng. Sci. **63**, 2829 (2008).
[10] C. Zhang, V. J. Pansare, R. K. Prud'homme, and R. D. Priestley, Soft Matter **8**, 86 (2012).
[11] A. Nikoubashman, V. E. Lee, C. Sosa, R. K. Prud'homme, R. D. Priestley, and A. Z. Panagiotopoulos, ACS Nano **10**, 1425 (2016).
[12] J. Q. Cui and I. Kretzschmarr, Langmuir **22**, 8281 (2006).
[13] A. Boker, J. He, T. Emrick, and T. P. Russell, Soft Matter **3**, 1231 (2007).
[14] C. E. Snyder, A. M. Yake, J. D. Feick, and D. Velegol, Langmuir **21**, 4813 (2005).
[15] A. M. Yake, C. E. Snyder, and D. Velegol, Langmuir **23**, 9069 (2007).
[16] K. Motoyoshi, A. Tajima, T. Higuchi, H. Yabu, and M. Shimomura, Soft Matter **6**, 1253 (2010).
[17] T. Higuchi, A. Tajima, H. Yabu, and M. Shimomura, Soft Matter **4**, 1302 (2008).
[18] H. Yabu, T. Higuchi, and M. Shimomura, Adv. Mater. **17**, 2062 (2005).
[19] T. Higuchi, A. Tajima, K. Motoyoshi, H. Yabu, and M. Shimomura, Angew. Chem. **120**, 8164 (2008).
[20] N. Li, A. Z. Panagiotopoulos, and A. Nikoubashman, Langmuir **33**, 6021 (2017).
[21] V. E. Lee, C. Sosa, R. Liu, R. K. Prud'homme, and R. D. Priestley, Langmuir **33**, 3444 (2017).
[22] C. Sosa, R. Liu, C. Tang, F. Qu, S. Niu, M. Z. Bazant, R. K. Prud'homme, and R. D. Priestley, Macromolecules **49**, 3580 (2016).
[23] C. Sosa, V. E. Lee, L. S. Grundy, M. J. Burroughs, R. Liu, R. K. Prud'homme, and R. D. Priestley, Langmuir **33**, 5835 (2017).
[24] N. Li, A. Nikoubashman, and A. Z. Panagiotopoulos, Soft Matter **13**, 8433 (2017).
[25] L. S. Grundy, V. E. Lee, N. Li, C. Sosa, W. D. Mulhearn, R. Liu, R. A. Register, A. Nikoubashman, R. K. Prud'homme, A. Z. Panagiotopoulos, and R. D. Priestley, ACS Nano **12**, 4660 (2018).
[26] J. C. Cheng, R. Vigil, and R. Fox, J. Colloid Interface Sci. **351**, 330 (2010).
[27] J. C. Cheng and R. Fox, Ind. Eng. Chem. Res. **49**, 10651 (2010).
[28] N. Di Pasquale, D. L. Marchisio, P. Carbone, and A. A. Barresi, Chem. Eng. Res. Des. **91**, 2275 (2013).
[29] A. D. Lavino, N. Di Pasquale, P. Carbone, and D. L. Marchisio, Chem. Eng. Sci. **171**, 485 (2017).
[30] D. T. Gillespie, J. Comput. Phys. **22**, 403 (1976).
[31] M. Thorn, H.-P. Breuer, F. Petruccione, and J. Honerkamp, Macromol. Theory Simul. **3**, 585 (1994).
[32] G. Odriozola, A. Moncho-Jordá, A. Schmitt, J. Callejas-Fernández, R. Martínez-García, and R. Hidalgo-Àlvarez, Europhys. Lett. **53**, 797 (2001).
[33] D. Mukherjee, C. G. Sonwane, and M. R. Zachariah, J. Chem. Phys. **119**, 3391 (2003).
[34] M. H. Flamm, T. Sinno, and S. L. Diamond, J. Chem. Phys. **134**, 034905 (2011).
[35] N. S. Tiwari and P. van der Schoot, J. Chem. Phys. **144**, 235101 (2016).
[36] P. G. Saffman and J. S. Turner, J. Fluid Mech. **1**, 16 (1956).
[37] M. V. Smoluchowski, Ann. Phys. **326**, 756 (1906).
[38] N. Fuchs, Z. Phys. **89**, 736 (1934).
[39] H. C. Hamaker, Physica **4**, 1058 (1937).
[40] J. Visser, Adv. Colloid Interface Sci. **3**, 331 (1972).
[41] S. Asakura and F. Oosawa, J. Chem. Phys. **22**, 1255 (1954).
[42] H. Yukawa, Proc. Phys.-Math. Soc. Jpn. **17**, 48 (1935).
[43] K. J. Ives, *The Scientific Basis of Flocculation* (Springer, Netherlands, 1978).
[44] V. E. Lee, personal communication (2018).
[45] B. K. Johnson and R. K. Prud'homme, Phys. Rev. Lett. **91**, 118302 (2003).
[46] R. F. Pagels, J. Edelstein, C. Tang, and R. K. Prud'homme, Nano Lett. **18**, 1139 (2018).